Pore formation kinetics in membranes, determined from the release of marker molecules out of liposomes or cells

Gerhard Schwarz and Charles H. Robert
Department of Biophysical Chemistry, Biocenter of the University, CH-4056 Basel, Switzerland

ABSTRACT We discuss the efflux of entrapped marker material from liposomes or cells through pores in the membrane, being monitored by the time course of a certain signal F (e.g., fluorescence emission). This is expressed in terms of an appropriate normalized function of time, the so-called efflux function $E(t)$. Under conditions frequently encountered in practice the measured $E(t)$ can be easily related to the forward rate of pore formation if the liposomes/cells are monodisperse in size. In the basic case of a time-independent rate law it turns out that $E(t)$ must be single exponential. Deviations from such a simple functional behavior might be due to a fairly broad distribution of liposome/cell sizes and/or a more complicated pore formation mechanism. A relevant evaluation of original data is demonstrated making use of experimental results obtained with small unilamellar lipid vesicles where pores are induced by the antibiotic peptide alamethicin. This includes the application of a general method to eliminate the effect of a given liposome/cell size distribution.

INTRODUCTION

Any solute marker material which is entrapped at higher concentration inside liposomes or biological cells tends to flow out into the surrounding medium once sufficiently large pores in the membrane are opened. Accordingly, measurements of this efflux process provide possibilities to demonstrate channel formation and to determine the associated kinetics. A special experimental procedure which has become quite popular takes advantage of a liposome- or cell-encapsulated self-quenching fluorescent dye which fluoresces when released (1). More recently this method has been employed to study the membrane action of colicin E1 (2), hemolysin (3), and tetanus toxin (4), respectively. We have begun using this technique to explore the rate of pore formation caused by the antibiotic peptide alamethicin (20 amino acids). The present article is primarily concerned with a theoretical analysis of pertinent data so that the underlying rate law can be established. Our approach is generally applicable to cases where the release of marker material through a sufficiently long-lived single pore is comparatively fast with regard to the overall efflux (see Appendix). A quantitative discussion of experiments with alamethicin acting on lipid vesicles is given as an illustration of the inherent potential for practical work.

Address correspondence to Dr. Gerhard Schwarz, Department of Biophysical Chemistry, Biocenter of the University, Klingelbergstrasse 70, CH-4056 Basel, Switzerland.

THEORETICAL

Efflux function and rate law

The marker substance (for example, a self-quenching fluorescent dye such as carboxyfluorescein or calcein) is envisaged to exhibit a signal F (e.g., an optical property such as fluorescent emission), changing between an initial value F_0 (for intact cells) and a final value F_∞, which is reached when all cells have been infected with pores and the efflux is thus complete. From the observed F in the measuring period we can determine a normalized efflux function,

$$E(t) = (F_\infty - F)/(F_\infty - F_0), \tag{1}$$

that describes the measured efflux in the course of time.

Initially, let us consider the cells (or liposomes) to be all of the same size but not necessarily spherical. The given internal cell volume is to be characterized by an equivalent spherical cell radius, R (corresponding to a sphere whose volume is equal to the actual volume of the cell interior). An additional basic parameter related to cell size is the number of lipid molecules, ν, in a single cell membrane. The total number of cells in the given system may then be expressed as

$$N = n_L N_A/\nu, \tag{2}$$

with n_L being the total amount (i.e., number of moles) of lipid in all the membranes (N_A, Avogadro's number).

Once a pore is opened in an individual cell membrane, a concentration gradient of marker molecules between the inner and outer bounds of that pore will result in a

0006-3495/90/09/577/07 $2.00

diffusion-mediated efflux of these molecules. A detailed analysis (see Appendix) reveals that this process will follow a single exponential time course. The relevant relaxation time τ_0 can often be much smaller than the time seen to elapse in the observed change of the signal F. Then the rate-limiting process will necessarily be the pore formation rather than the diffusion of marker material flowing out of the cells. These cases are of practical interest and will be investigated here with regard to pores having sufficiently long lifetimes ($\gg \tau_0$) so that the very first pore formed in a cell membrane gives rise to essentially complete release of the encapsulated marker substance (to the level of its external concentration).

Under these circumstances we consider the situation evolving after a pore forming agent is added to a suspension of N individual cells. Let N_i be the number of cells infected with i pores ($i = 0, 1, 2, \ldots$) after a time t. Since the total number of pores a given cell could experience is very large, the N_i are evidently subject to a Poisson probability distribution. Thus, in particular, the number of intact cells (no pores) becomes $N_0 = N \cdot \exp(-p)$, where $p(t)$ is the average number of pores so far ever formed per cell. All the other cells ($i \geq 1$) will be clear of the marker material due to the fast efflux once a pore is formed. Since they are all of the same size, each cell contributes the same share to the change of F, and the efflux function is simply equal to N_0/N, or

$$E(t) = e^{-p(t)}. \tag{3}$$

The accordingly defined pore number $p(t)$ can be readily related to the forward rate of pore formation, defined by

$$v_p = (dr_p/dt)_{\text{forward}}. \tag{4a}$$

The quantity $r_p = n_p/n_L$ (molar ratio of pores per lipid) is chosen as the appropriate concentration variable for pores in the membrane. The reverse rate (describing inactivation of pores) will naturally be irrelevant because the measured signal is not affected when a pore eventually gets closed. Integration of Eq. 4a and division by N (see Eq. 2) results in the general relation

$$p(t) = \nu \cdot \int_0^t v_p \cdot dt. \tag{4b}$$

This pore number function can be readily determined from the experimental efflux function. According to Eq. 3 a plot of $-\ln E(t)$ vs. t directly leads to $p(t)$. The slope of this curve

$$dp/dt = \nu \cdot v_p \tag{5a}$$

reflects the actual forward rate of pore formation at the given instant of time. The initial slope may be used to define a first-order rate constant related to single vesicles of uniform size

$$k_0 = (dp/dt)_{t=0} = \nu \cdot v_p^0, \tag{5b}$$

measuring the rate at the very beginning of the experiment.

Basic mechanism

If v_p remains constant during the whole period of measurable changes of F (i.e., up to p values of ~3–4), we simply have

$$E(t) = \exp(-k_0 t). \tag{6}$$

In other words, the observed release of marker material is subject to a single exponential time function. This can be expected to apply in the case of the following basic model mechanism. A pore-forming substance B is hypothesized to associate very rapidly with the membrane and then to turn slowly into pores as expressed by the reaction scheme

$$B_f \overset{\text{(fast)}}{\rightleftharpoons} B_a, \quad m \cdot B_a \xrightarrow{k_p} P \tag{7a}$$

It involves the free (i.e., nonassociated) and associated monomeric states, B_f and B_a, respectively. P is an open pore composed of m monomers. The k_p stands for a rate constant according to a possible nth order rate law ($n \leq m$),

$$v_p = k_p \cdot r_a^n \tag{7b}$$

(r_a, molar ratio of B_a per lipid). We assume the number of open pores to be always much smaller than the number of B_a molecules. Then r_a will reach a constant value almost immediately by virtue of the fast partitioning equilibrium $B_f \rightleftharpoons B_a$ resulting in $r_a = (\Gamma/\alpha) \cdot c_f$, where c_f is the concentration of B_f, and Γ stands for an appropriate partition coefficient; possible nonideal interactions of B_a are described by the activity coefficient α (5). Owing to mass conservation we have $c_f + r_a c_L = c_B$ (c_L, lipid concentration; c_B, total concentration of B) and can therefore readily calculate r_a in terms of c_B and c_L. So one arrives at a single exponential efflux function as formulated in Eq. 6, where now

$$k_0 = \nu k_p' \cdot c_B^n, \quad k_p' = k_p \cdot [\Gamma/(\alpha + \Gamma c_L)]^n. \tag{8}$$

This will be strictly proportional to c_B^n as long as mutual interactions of B_a can be neglected ($\alpha \approx 1$).

Effect of cell size distribution

In case the efflux function is found to be not single exponential, in other words, if appreciable curvature is seen when $-\ln E(t)$ is plotted vs. t, a more complicated

mechanism of pore formation may be indicated. One must take into account, however, that some curvature will be caused by a distribution of cell sizes. Larger cells naturally have a better *a priori* chance to be infected by an open pore and so will lose their marker material sooner than smaller cells.

The fraction of cells having an inner radius between R and $R + dR$ may be given as $\varphi(R)\,dR$. The number of lipid molecules per cell, ν, and possibly also v_p depend on R. This generally implies the existence of a specific pore number function $p(R, t)$. The amount of marker substance contributing to F is proportional to R^3. Then, the actually measured efflux function becomes

$$E(t) = \int_0^\infty R^3 \cdot e^{-p(R,t)} \cdot \varphi(R) \cdot dR \Big/ \int_0^\infty R^3 \cdot \varphi(R) \cdot dR, \tag{9a}$$

which is the proper average of the basic efflux function in Eq. 3.

For practical reasons, let us describe the size distribution in terms of the dimensionless variable $x = R/R_0$ with regard to some arbitrary reference radius R_0. Cells with this radius have the pore number function $p_0(t)$. According to Eq. 4b we can generally express $p(R, t)$ as $p_0(t)$ multiplied by the scaling factors $w(x) = \nu/\nu_0$ and $v(x) = v_p/(v_p)_0$. We may then convert Eq. 9a to

$$E(t) = \int_0^\infty x^3 \exp\left[-w(x) \cdot v(x) \cdot p_0(t)\right]\varphi_0(x)dx \Big/ \int_0^\infty x^3\varphi_0(x)\,dx. \tag{9b}$$

The size distribution function is denoted $\varphi_0(x)$. First we consider a rate law being independent of cell size, i.e., $v(x) = 1$, and set $w(x) = x^2$, which is expected to be applicable to larger cells of fairly spherical shape (because ν would be proportional to the membrane surface). Then for a rectangular size distribution up to $R = R_0$ (implying there are no cells with $R > R_0$), Eq. 9b is readily integrated, yielding the simple expression,

$$E(t) = 2 \cdot [1 - (1 + p_0)e^{-p_0}]/p_0^2 = 1 - (2/3)p_0 + (1/4) \cdot p_0^2 - \ldots \tag{10a}$$

Let us compare this size-averaged efflux function with the efflux function $\overline{E}(t)$ of a hypothetical monodisperse cell suspension with a certain mean radius $\overline{R}$. Expanding Eq. 3, we have $\overline{E}(t) = \exp[-\overline{p}(t)] = 1 - \overline{p} + (1/2)\overline{p}^2 \ldots$, where $\overline{p}(t)$ is the proper pore number function for that mean radius. We now define $\overline{R}$ as the uniform cell radius for which the corresponding $\overline{E}(t)$ will have the same initial slope as the actual size-averaged $E(t)$. It follows from Eq. 10a that we must set

$$(2/3)p_0(t) = (\overline{R}/R_0)^2\, p_0(t) = \overline{p}(t), \tag{10b}$$

owing to our basic assumption of $p(R, t)$ being proportional to R^2. In the present case we thus arrive at an apparent mean $\overline{R} = \sqrt{2/3} \cdot R_0$.

To analyze effects of size distribution effects on a measured efflux function, we first define an apparent average pore number

$$p^*(t) = -\ln E(t). \tag{11}$$

For the circumstances of the above rectangular $\varphi(R)$, this quantity can be calculated readily from Eq. 10a and plotted vs. the respective $\overline{p}(t)$ as shown in Fig. 1. If all the cells had actually the same radius $R = \overline{R}$, the analogous plot would naturally be the trivial straight line $p^* = \overline{p}$. For any given $\varphi(R)$ and $w(x)$, $v(x)$ functions we may calculate specific p^* vs. $\overline{p}$ curves (for further details see Appendix).

We are now in a position to eliminate the effect of size distribution on the experimental data. For any of the apparent $p^*(t)$ taken from the measured $E(t)$, a pertinent $\overline{p}$ value is determined by means of the specific p^* vs. $\overline{p}$

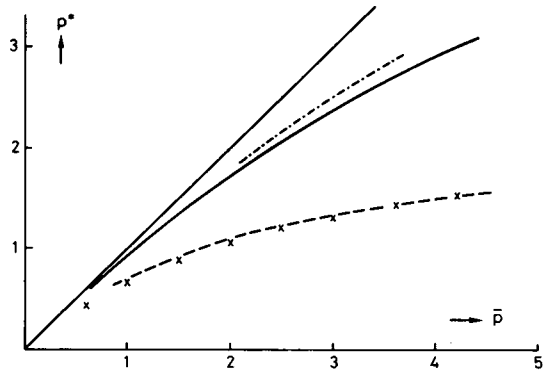

FIGURE 1 Dependence of the apparent number of pores per cell p^* on the mean $\overline{p}$ (see text). The straight line represents the trivial case of uniform cell sizes. The other curves refer to a rectangular distribution of spherical cell sizes with the inner radius R covering the range from 0 through an upper bound R_0 (see Appendix for details). The solid curve has been calculated for a size-independent pore formation rate v_p and a cell surface being proportional to R^2 (Eq. 10). The dashed and dotted curve results from a more rigorous calculation which takes into account the given finite value of the bilayer thickness relative to the cell diameter (ν as in Eq. A3). The dashed curve considers a size-dependent value of v_p which is proportional to R^5. Conversion of an experimental p^* value (e.g., $p^* = 2.0$ at $t = 4.2$ min for the 0.55 μM experiment in Fig. 3) into a $\overline{p}$ value applying to a certain mean cell size (of radius $\overline{R}$) can be carried out as follows. First, one has to choose the appropriate curve derived for the underlying size distribution function and radius dependence of the pore number p. For example, with the given solid curve, $p^* = 2.0$ is apparently equivalent to a $\overline{p} = 2.4$ (see dashed arrow in Fig. 3). This is the average number of pores formed within 4.2 min in a cell of radius $\overline{R}$. As noted in the text, in order to convert our experimental $p^*(t)$ into a $\overline{p}(t)$ with a constant slope, a particular p^* vs. $\overline{p}$ curve is required that fits the points indicated by the crosses. Evidently this is quite well achieved by the dashed curve.

curve that was calculated for the given size distribution and appropriate $w(x)$, $v(x)$. The original $p^*(t)$ can so eventually be transformed in a function $\bar{p}(t)$ which refers to the pore opening rate of cells having the pertinent mean radius $\bar{R}$. The procedure will be practically demonstrated below.

EXPERIMENTAL

Materials and methods

We have studied the efflux of the self-quenching dye 5(6)-carboxyfluorescein (CF) from unilamellar vesicles of palmitoyloleoylphosphatidylcholine (POPC), induced by the pore forming antibiotic peptide alamethicin. The CF was supplied by Sigma Chemical Co. (St. Louis, MO), the POPC by Avanti Polar Lipids, Inc. (Birmingham, AL). Preparation and characterization of the peptide has been described previously (6). The vesicles were made by sonification in 50 mM dye and separated from free dye by passing the solution over a Sephadex G50 column (1). Experiments were conducted at 20°C and pH 7.4 (Tris buffer). In each efflux experiment a 10-μl amount of a vesicle stock solution (≈5–8 mg/ml lipid) was added to a 3-ml quartz cuvette containing a particular solution of the peptide, which is stirred continuously. With a series 8000 fluorometer (SLM Instruments, Inc., Urbana-Champaign, IL) an increase of fluorescence emission, F, in the course of time is observed. This presumably arises from the relief of quenching of the CF when the dye inside the vesicles is released into the external bulk medium where its concentration is very much reduced. We recorded some very slow leakage of dye which occurs even with no peptide added.

It should be emphasized that titrating vesicles with peptide is not advisable. Preliminary experiments done in this way result in very fast initial efflux rates which were ill defined. These effects presumably are due to transient high local concentrations of the peptide in that part of the solution where the stock peptide solution is injected. Because pore formation is greatly dependent upon the concentration of alamethicin, substantial errors are introduced particularly at the start of the experiments before stirring can establish a homogeneous concentration of the pore former.

The distribution of vesicle sizes was investigated with negative stain electron microscopy on a preparation of sonicated vesicles made in essentially the same way as for the efflux experiments.

RESULTS

Measured F for three alamethicin concentrations in the 0.25–0.55 μM range are given in Fig. 2. The "infinite time" signal F_∞ was ascertained after addition of a detergent (Triton X-100) which destroys the vesicles. The value F_0, on the other hand, could be determined by extrapolation. Having evaluated the efflux function $E(t)$ as defined in Eq. 1, the apparent $p^*(t)$ according to Eq. 11 was evaluated for each concentration (see Fig. 3). These raw data were then processed to eliminate the effects of vesicle size and background leakage.

The histogram of vesicle sizes is shown in Fig. 4. It can be approximated by a rectangular distribution of inner vesicle radii varying up to $R_0 = 182$ Å (neglecting the lower bound; see Appendix). The appropriate mean

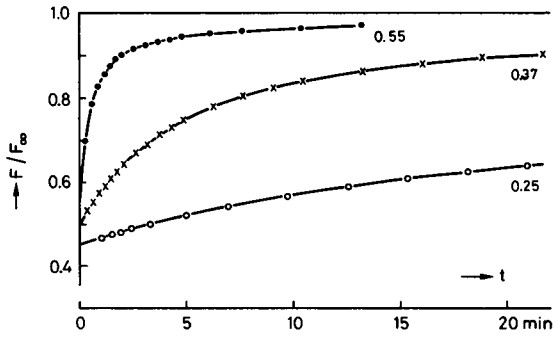

FIGURE 2 Fluorescence emission F at 425 nm (390 nm excitation) relative to F_∞ (at completed efflux) measured as a function of time for three alamethicin concentrations (given in micromolars).

radius according to Eq. 10b becomes $\bar{R} = 149$ Å. Assuming a size-independent pore formation rate v_p, we applied the procedure described above to determine $\bar{p}(t)$ for this special vesicle size and eventually corrected the results for spontaneous leakage (determined as $5 \cdot 10^{-3}$ pores per minute). The final curves are exhibited in Fig. 3 for the two larger peptide concentrations. The initial slope, $(d\bar{p}/dt)_0$, is found to depend on the aqueous alamethicin concentration with a power of ~5.5, as demonstrated in Fig. 5.

DISCUSSION

Alamethicin has been intensively studied regarding its ability to induce voltage-gated conductance in planar

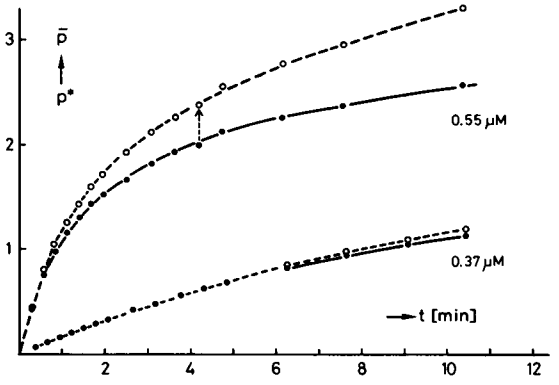

FIGURE 3 (*Solid circles*) Apparent p^* according to the data of Fig. 2 (for alamethicin concentrations 0.55 and 0.37 μM). (*Open circles*) Leakage corrected $p(t)$ for a mean vesicle radius ($\bar{R} = 149$ Å) taking into account a rectangular size distribution up to $R = 182$ Å (see Appendix for arguments) and a size-independent v_p. For the method of converting p^* to $\bar{p}$ see Fig. 1 (dashed arrow refers to the numerical example mentioned there).

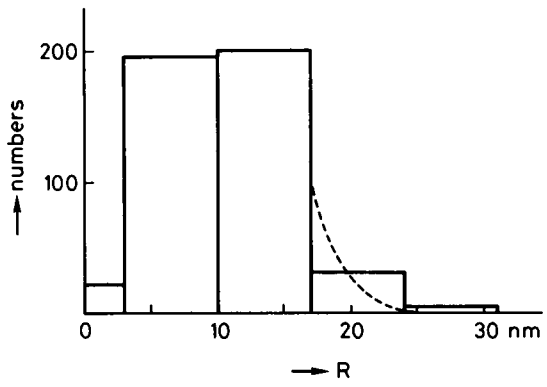

FIGURE 4 Histogram of vesicle size distribution in our samples. Numbers of vesicles counted (under the electron microscope) which fall with their inner radius R in the given bins. The dashed curve gives a more realistic approximation of the distribution above 170 Å. It represents the function $100 \cdot \exp(1 - x^2)$, where $x = R/170$ Å. Together with a rectangular distribution up to $R = 170$ Å this was used to calculate the modified p^* vs. $\bar{p}$ curve mentioned in the Appendix.

lipid bilayers (7–10). This phenomenon is attributed to pore formation involving aggregation of incorporated peptide monomers. The estimated pore diameters of 10–25 Å (7) are large enough to permit diffusional passage of carboxyfluorescein molecules, which have an approximate diameter of 10 Å (derived from the molecular weight of 378). We can expect that such pores will also be formed in our vesicle preparations under zero-voltage conditions (preliminary experiments with a diffusion potential being positive outside have resulted in faster

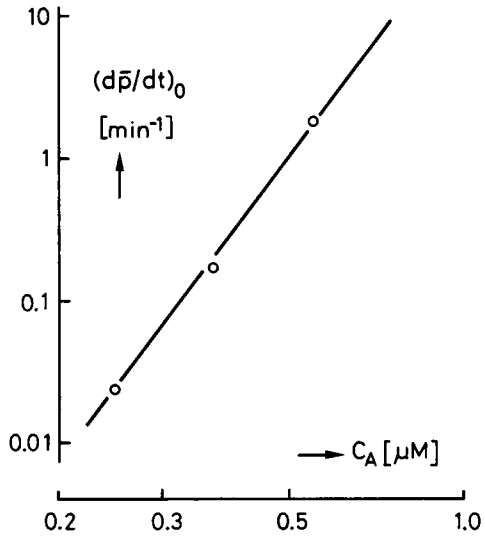

FIGURE 5 Double logarithmic plot of the mean initial rate $(d\bar{p}/dt)_0$ vs. alamethicin concentration c_A, for a size-independent pore formation rate. The slope is equal to 5.5.

efflux rates). The lifetime of an open pore is of the order of 10 ms or more (9, 11) which is much longer than the τ_0 value of <1 ms calculated for the relaxation time of CF efflux through a single pore in the vesicle membrane (see Appendix). Therefore, the condition of full depletion of the dye by the very first pore is apparently met so that the measured efflux functions can be related to the forward rate of pore formation as pointed out above.

The apparent pore numbers per vesicle, $p^*(t) = -\ln E(t)$, presented in Fig. 3 are averages over the given vesicle size distribution. We can convert them to $\bar{p}$ values describing the pore formation rate in a vesicle having an appropriate mean radius $\bar{R}$ by making use of theoretical curves as drawn in Fig. 1 (for more details see Appendix). Let us first consider a rate ν_p, which is independent of vesicle size. Then we obtain the corrected curves of Fig. 3 applying to an inner radius of 149 Å. Their slopes become smaller and smaller in the course of time. This indicates a gradual decrease of ν_p. Let us examine a possible mechanism.

It has been shown previously (12) that the partitioning of alamethicin between the aqueous and bilayer media takes place in <1 s. Therefore, we have in fact a very fast equilibration of associated and free peptide monomers as indicated in the basic reaction scheme of Eq. 7. The rate-limiting step must occur in the aggregation process. Most simply we may imagine that in a series of individual steps a decisive intermediate aggregate A_{n+1} (of $n + 1$ monomers) is eventually formed which is the final stable nucleus turned immediately into an active pore P. In particular, the following reactions are to be envisaged:

$$A_{n-1} + A_1 \underset{k_{-n}}{\overset{k_n}{\rightleftharpoons}} A_n, \quad A_n + A_1 \xrightarrow{k_{n+1}} A_{n+1} \overset{\text{(fast)}}{\dashrightarrow} P, \qquad \text{(11a)}$$

where the reverse step towards A_n can be neglected. Then, of course,

$$\nu_p = k_{n+1} \cdot r_1 \cdot r_n. \qquad \text{(11b)}$$

Assuming a steady-state condition for A_n, we obtain

$$r_n = k_n \cdot r_1 \cdot r_{n-1}/(k_{-n} + k_{n+1} \cdot r_1). \qquad \text{(11c)}$$

This can be readily expressed in terms of the associated monomer concentration, r_1, if a fast preequilibrium of A_{n-1} with the A_1 is taken into account (K_{n-1} being the appropriate equilibrium constant). Then Eq. 11b leads to

$$\nu_p = k_n \cdot K_{n-1} \cdot \frac{k_{n+1} \cdot r_1}{k_{-n} + k_{n+1} \cdot r_1} \cdot r_1^n. \qquad \text{(11d)}$$

This rate law in terms of r_1 would reflect an order between n (for $k_{n+1} \cdot r_1 \gg k_{-n}$) and $n + 1$ (for $k_{n+1} \cdot r_1 \ll k_{-n}$). The same order is expected with respect to the total alamethicin concentration c_A, owing to the existence of a fast partitioning of the free and associated peptide mono-

mers. Our results for $(d\bar{p}/dt)_0$ in Fig. 5 could accordingly be explained on the basis of a pore nucleus of six monomers. This refers, however, to the initial phase of the measured efflux only. To understand a drastic slowing down of v_p at later times with the simple scheme 11a, a substantial decrease of r_1 (and of the free alamethicin concentration as well) in the range of minutes would be necessary. However, such a phenomenon has never been observed in appropriate titration and kinetic experiments (6, 12). Moreover, it should be noted that the total amount of lipid in these experiments is insufficient to appreciably deplete the aqueous solution phase, given a partition coefficient of the order of 10^3 M^{-1} (6). Thus r_1 is actually buffered due to the fast partitioning.

An alternative possibility is that the decrease of v_p may be brought about by a possible side reaction of A_n resulting in irreversible nonpore aggregates. One could propose a slowly evolving structural alternative (composed of one or more peptide monomers) which can react with A_n so that the rate-limiting, steady-state value of r_n (see Eq. 11b) is reduced.

One may raise the question that there might be an effect of cell size (or bilayer curvature, respectively) on the rate of pore formation (v_p) in contrast to our original assumption. Because in the course of the efflux process the larger vesicles will be depleted most rapidly, the apparent $\bar{p}(t)$ of Fig. 3 will naturally reflect the v_p at a gradually decreasing vesicle size. A time-independent value of v_p for a fixed radius R can in fact be reconciled with our data if a particular p^* vs. $\bar{p}$ dependence is hypothesized as indicated by the crosses in Fig. 1. It is very well fitted by a theoretical curve assuming v_p to be proportional to R^5 in the given range of vesicle sizes (see Appendix). The underlying R^5 dependence of v_p could possibly reflect a partition coefficient Γ which increases about linearly with R as can be inferred from Eq. 8. However, when measured Γ for the highly curved bilayers of small vesicles have been compared with those for the relatively flat bilayer structures of coarse lipid dispersions, no significant change could be noticed (13).

Thus a gradual inactivation of the pore formation rate may be the more likely cause of the decrease of slope in our $\bar{p}(t)$ curves. This appears to be in line with observations that in planar lipid membrane experiments the alamethicin-induced conductance runs through a maximum within 3–6 min after having added the peptide, and then declines to a steady-state value over the next 25–30 min (14). Moreover, we have preliminary efflux data obtained for an approximately monodisperse suspension of large vesicles (≈100 nm diameter) which still reflect a definite decrease of v_p in the course of time (Zong, R., C. H. Robert, and G. Schwarz, unpublished results). Further work to clarify these points is in progress.

APPENDIX

Efflux through a single pore

Diffusion-mediated flow of marker molecules through an open pore can be described according to Fick's first law, namely,

$$-(dn/dt) = A_p \cdot D_m(c - c')/d, \qquad \text{(A1)}$$

with n being the amount (mol number) of the marker material at time t inside a given cell, c and c' standing for the internal and external concentrations, respectively, at the pore bounds (A_p, effective cross-section of the pore; D_o, diffusion coefficient of marker molecules in the pore; d, pore length = thickness of the membrane). It is assumed that the intracellular concentration equilibrates sufficiently fast so that $n = (4\pi/3) \cdot R^3 \cdot c$; c' can be taken as a constant. Under these circumstances Eq. A1 is easily solved, resulting in

$$c - c' = (c_o - c') \cdot \exp^{-t/\tau_o} \qquad \text{(A2a)}$$

(c_o, given value of c_o at $t = 0$), reflecting the intrinsic release time,

$$\tau_o = (4\pi/3) \cdot R^3 d/A_p D_o. \qquad \text{(A2b)}$$

In the case of marker ions, the pertinent pore conductance may be introduced to express d/A_pD_o (15). For a discussion of the actual time scales we set $d = 4$ nm (16), $A_p = 0.3$ nm^2, and $D_o = 5 \cdot 10^{-6}$ cm^2/s (equivalent to a Stokes radius of 0.5 nm in an aqueous medium). Small unilamellar lipid vesicles with $R \leq 20$ nm then would release their marker material at a rate characterized by $\tau_o \leq 1$ ms. A constant concentration gradient in the pore as implied by Eq. A1 is in fact established very much faster ($d^2/2D_o \approx 10^{-8}$ s). The time scale for reequilibrating any change of internal concentration is expected to be in the range of $R^2/6D_o \approx 10^{-7}$ s. A constant level of c' outside the cell is maintained because the solution is continuously stirred during our measurements. Accordingly, the conditions for the above solution of Eq. A1 are certainly met. It must be emphasized, however, that τ_o tends to assume fairly large values when the radius increases. According to the R^3 dependence in Eq. A2b a radius of 2 μm for instance would imply a τ_o of some 15 min. Therefore, the release of marker material may possibly be complicated by a competition between diffusion through a single open pore and the overall pore formation kinetics. In that case a more sophisticated theoretical analysis than the present one will be required.

Aspects of vesicle size distribution

Our lipid vesicle system has been found to involve a broad range of radii R. This will certainly affect $p(t)$ because of the factor ν, the number of lipid molecules per vesicle (see Eq. 4b). The latter can readily be expressed as

$$\nu = 4\pi[(R + d)^2/A'_L + R^2/A''_L] \qquad \text{(A3)}$$

(A'_L and A''_L are area per lipid molecule in outer and inner surface of the membrane). For our mean vesicle size of $\bar{R} = 149$ Å, this yields $\bar{\nu} = 1.06 \cdot 10^4$ lipid molecules if the values $A'_L = 74$ Å^2, $A''_L = 61$ Å^2 for phosphatidylcholines (16) are used.

We have approximated our size distribution data as given in Fig. 4 by a rectangular distribution function with lower and upper bounds of $R = 22$ and 182 Å, respectively. It turned out that the averaging procedure according to Eq. 9 was practically insensitive to very small values of R. So we could simply start the integration at $R = 0$. Assuming a size-independent v_p implies $v(x) = 1$ in Eq. 9b. The other scaling function $w(x)$ becomes a quadratic function as derived from Eq. A3. Under these circumstances the dashed-dotted curve in Fig. 1 is obtained.

It is, however, suspected to underestimate the contribution of the larger vesicles in the bin at radii of 170 through 240 Å. In view of the fact that the actual distribution of vesicle sizes is more Gaussian than rectangular (17) we have modified our approximation appropriately above 170 Å as shown by the dashed tail in Fig. 4. The resulting p^* vs. $\bar{p}$ curve is found to be practically the same as for a strictly rectangular distribution where we set in Eq. 9b $w(x) = x^2$ and $v(x) = 1$. This can be readily integrated in a closed form (see Eq. 10a) and is presented as the solid curve in Fig. 1. We actually used this to convert our p^* to $\bar{p}$ (see Fig. 3).

Once we give up the presumption of a size-independent rate law, substantial changes in the p^* vs. $\bar{p}$ dependences may be generated. With a v_p proportional to R^5, i.e., $v(x) = x^5$, the dashed curve in Fig. 1 will be applicable. This in fact converts our measured p^* curves into $\bar{p}(t)$, which increase linearly with time (and refers to an appropriate mean radius of $\bar{R} = 158$ Å).

We thank Dr. S. Stankowski for stimulating discussions and useful advice as well as Edwin Kalb for performing the negative stain EM procedures.

This work was supported by grants No. 3.285.85/3.25230.88 from the Swiss National Science Foundation and by the North Atlantic Treaty Organization (fellowship to C.H.R.).

Received for publication 7 March 1990 and in final form 1 May 1990.

REFERENCES

1. Weinstein, J. N., S. Yoshikami, P. Henkart, R. Blumenthal, and W. A. Hagins. 1977. Liposome-cell interaction. Transfer and intracellular release of a trapped fluorescent marker. *Science (Wash. DC)*. 195:489–492.
2. Kayalar, C., and N. Düzgünes. 1986. Membrane action of colicin E1. Detection by the release of carboxyfluorescein and calcein from liposomes. *Biochim. Biophys. Acta*. 860:51–56.
3. Menestrina, G. 1988. Escherichia coli hemolysin permeabilizes small unilamellar vesicles loaded with calcein by a single-hit mechanism. *FEBS (Fed. Eur. Biochem. Soc.) Lett*. 232:217–220.
4. Menestrina, G., S. Forti, and F. Gambale. 1989. Interaction of tetanus toxin with lipid vesicles. Effects of pH, surface charge, and transmembrane potential on the kinetics of channel formation. *Biophys. J.* 55:393–405.
5. Schwarz, G., S. Stankowski, and V. Rizzo. 1986. Thermodynamic analysis of incorporation and aggregation in a membrane: application to the pore-forming peptide alamethicin. *Biochim. Biophys. Acta*. 861:141–151.
6. Rizzo, V., S. Stankowski, and G. Schwarz. 1987. Alamethicin incorporation in lipid bilayers. A thermodynamic study. *Biochemistry*. 26:2751–2759.
7. Eisenberg, M., J. E. Hall, and C. A. Mead. 1973. The nature of the voltage-dependent conductance induced by alamethin in black lipid membranes. *J. Membr. Biol*. 14:143–176.
8. Gordon, L. G. M., and D. A. Haydon. 1975. Potential-dependent conductances in lipid membranes containing alamethicin. *Philos. Trans. R. Soc. Lond. B. Biol. Sci*. 270:433–447.
9. Boheim, G., and H. A. Kolb. 1978. Analysis of the multi-pore system of alamethicin in a lipid membrane. *J. Membr. Biol*. 38:99–191.
10. Hall, J. E., I. Vodyanoy, T. M. Balasubramamian, and G. R. Marshall. 1984. Alamethicin, a rich model for channel behavior. *Biophys. J*. 45:233–247.
11. Boheim, G. 1974. Statistical analysis of alamethicin channels in black lipid membranes. *J. Membr. Biol*. 19:277–303.
12. Schwarz, G., H. Gerke, V. Rizzo, and S. Stankowski. 1987. Incorporation kinetics in a membrane, studied with the pore-forming peptide alamethicin. *Biophys. J*. 52:685–692.
13. Stankowski, S., and G. Schwarz. 1989. Lipid-dependence of peptide-membrane interactions. Bilayer affinity and aggregation of the peptide alamethicin. *FEBS (Fed. Eur. Biochem. Soc.) Lett*. 250:556–560.
14. Vodyanoy, I., J. E. Hall, and V. Vodyanoy. 1988. Aggregation of alamethicin molecules in the planar lipid bilayer. *Biophys. J*. 53:514a. (Abstr.)
15. Miller, C. 1984. Ion channels in liposomes. *Annu. Rev. Physiol*. 46:549–558.
16. Huang, C., and J. T. Mason. 1978. Geometric packing constraints in egg phosphatidylcholine vesicles. *Proc. Natl. Acad. Sci. USA*. 75:308–310.
17. Stelzer, E., and H. Ruf. 1983. Characterisation of phospholipid vesicles by photon correlation spectroscopy enabling the detailed analysis of transport parameters. *In* Physical Chemistry of Transmembrane Ion Motions. G. Spach, editor. Elsevier Science Publishers B. V., Amsterdam. 37–43.